

# Enhancing Deep Reinforcement Learning-based Robot Navigation Generalization through Scenario Augmentation

Shanze Wang<sup>1,2†</sup>, Mingao Tan<sup>2†</sup>, Zhibo Yang<sup>3</sup>, Xianghui Wang<sup>2</sup>, Xiaoyu Shen<sup>2</sup>,  
Hailong Huang<sup>1</sup> and Wei Zhang<sup>2</sup>

**Abstract**—This work focuses on enhancing the generalization performance of deep reinforcement learning-based robot navigation in unseen environments. We present a novel data augmentation approach called scenario augmentation, which enables robots to navigate effectively across diverse settings without altering the training scenario. The method operates by mapping the robot’s observation into an imagined space, generating an imagined action based on this transformed observation, and then remapping this action back to the real action executed in simulation. Through scenario augmentation, we conduct extensive comparative experiments to investigate the underlying causes of suboptimal navigation behaviors in unseen environments. Our analysis indicates that limited training scenarios represent the primary factor behind these undesired behaviors. Experimental results confirm that scenario augmentation substantially enhances the generalization capabilities of deep reinforcement learning-based navigation systems. The improved navigation framework demonstrates exceptional performance by producing near-optimal trajectories with significantly reduced navigation time in real-world applications.

## I. INTRODUCTION

Autonomous navigation is important for mobile robots, with SLAM efficiently handling known environments [1]. However, in unknown or dynamic settings, unreliable maps limit traditional methods, necessitating mapless navigation based on local perception [2]. Learning-based approaches using deep neural networks [3] generate motion commands directly from sensor data, bypassing intermediate processes while handling high-dimensional inputs with computational efficiency even on modest hardware [4].

Deep Reinforcement Learning (DRL) [5] leads among learning-based navigation methods, with agents optimizing

This work has been submitted to the IEEE for possible publication. Copyright may be transferred without notice, after which this version may no longer be accessible.

\*This work is supported by 2035 Key Research and Development Program of Ningbo City under Grant No.2024Z127. (Corresponding author: Wei Zhang.)

<sup>1</sup>Shanze Wang and Hailong Huang are with the Department of Aeronautical and Aviation Engineering, Hong Kong Polytechnic University. shanze.wang@connect.polyu.hk; hailong.huang@polyu.edu.hk.

<sup>2</sup>Shanze Wang, Mingao Tan, Xianghui Wang, Xiaoyu Shen and Wei Zhang are with the Ningbo Key Laboratory of Spatial Intelligence and Digital Derivative, Institute of Digital Twin, Eastern Institute of Technology, Ningbo, China. szwang@eitech.edu.cn; mtan@eitech.edu.cn; xhwang@eitech.edu.cn; xyshen@eitech.edu.cn; zh@eitech.edu.cn.

<sup>3</sup>Zhibo Yang is with the Department of Mechanical Engineering, National University of Singapore. zhibo.yang@u.nus.edu

<sup>†</sup>These authors contributed equally to this work as co-first authors.

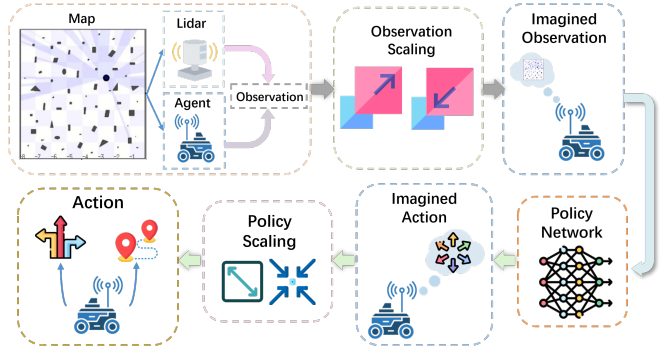


Fig. 1. The framework of proposed scenario augmentation method.

behavior through environmental interactions and reward signals. DRL surpasses imitation learning in robustness without requiring expert demonstrations [6]. While physical training presents resource and safety challenges, simulation offers a practical alternative. Advanced simulators with simulation-to-reality techniques [7] enable effective policy transfer to real-world systems, particularly for robots with distance sensors. Existing research predominantly focuses on optimizing navigation performance within training environments [8], [9], [10], yielding favorable outcomes when test conditions mirror training scenarios [11]. However, significant performance degradation occurs in novel environments, where DRL agents exhibit undesired behaviors [8], [10]. Current DRL navigation approaches typically employ a severely constrained set of training environments [12], with most studies limiting training to either one [11] or two [9], [10] carefully designed scenarios. While enhancing environmental diversity improves generalization capabilities [13], it simultaneously increases computational demands, highlighting the need for resource-efficient generalization methods [14]. This generalization challenge [15] arises when real-world observations diverge substantially from training data, compromising the agent’s ability to transfer learned behaviors to new situations.

This paper presents scenario augmentation, a computationally efficient data augmentation method that generates diverse training scenarios without modifying the physical environment layout. Through systematic analysis, we identify insufficient training scenario diversity as the primary factor in performance degradation. Experimental results confirm that scenario augmentation significantly enhances the generalization capability of DRL navigation agents. The main contributions of this paper are:

- A novel scenario augmentation method that improves DRL navigation agents’ generalization by creating dynamic mappings between real and imagined spaces, enabling diverse training experiences while maintaining the same physical environment.
- Comprehensive experimental validation across multiple simulated and real-world environments, demonstrating the method’s effectiveness and robustness in both complex static settings and dynamic pedestrian scenarios.

## II. RELATED WORKS

Deep Reinforcement Learning (DRL) enables adaptive learning in dynamic environments [16] and optimizes complex, high-dimensional policies, thus enhancing navigation efficiency and robustness. Although algorithms such as DQN [17], PPO [18], and SAC [19] have been widely implemented, they are not specifically designed for mapless navigation tasks [20]. Consequently, they may encounter challenges such as sparse rewards and limited generalization in complex, crowded environments.

The capacity for generalization in DRL becomes paramount when testing environments differ from training environments. Navigation agents are prone to overfitting, which may result in suboptimal decisions in unfamiliar settings [21]. Various techniques have been explored to improve DRL generalization, with research predominantly focusing on addressing overfitting to restricted observations and adapting to new environments [22].

Researchers have proposed various approaches to navigation challenges. Yang et al. [23] enhanced safe navigation in crowded environments using deep reinforcement learning with a local risk map that captured human interactions. Reinis et al. [24] developed a system that selected optimal waypoints and integrated learned motion policies for navigation without prior maps in both static and dynamic environments. Xie et al. [25] created a control strategy combining LiDAR data, pedestrian kinematics, and subgoal points to generate steering and velocity commands.

Studies have shown that neural networks favor simple functions, potentially limiting their effectiveness in reinforcement learning tasks [26]. The bias toward smooth functions can negatively impact value approximation in DRL [27]. Yang et al. [28] and Brellmann et al. [29] proposed adjusting Fourier feature scales to capture high-frequency components, though this approach risks fitting noise and reducing generalization capability with limited training data.

Imitation learning accelerates DRL training [2] but requires significant design effort. Shi et al. [11] and Cai et al. [30] improved training efficiency using intrinsic and unrelated rewards, though generalization to novel scenarios remains uncertain. Raileanu and Fergus [31] found that decoupling value approximation and policy networks improves generalization, despite increased computational demands and potential training instability.

## III. PROBLEM FORMULATION

Goal-driven robot navigation can be discretized into a sequential decision-making process. As illustrated in Fig.

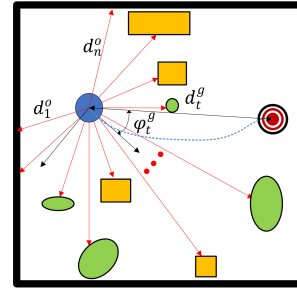


Fig. 2. Illustration of the goal-driven robot navigation problem.

2, the robot’s task is to reach its designated goal while successfully navigating around obstacles. The goal’s relative position  $s_t^g = \{d_t^g, \varphi_t^g\}$  is determined using either pre-existing maps or localization sensors, including WIFI and microphone arrays. The system employs a DNN controller parameterized by  $\theta$ , which implements a control policy  $\pi_\theta$ . The controller accepts input  $s_t = \{s_t^g, s_t^o\}$ , where  $s_t^o$  denotes local environmental data acquired through 2D Lidar scans. The Lidar sensor’s coordinate frame coincides with the robot’s local reference frame, centered between the drive wheels. At time step  $t$ , the policy  $\pi_\theta$  generates velocities  $a_t = \{v_t, \omega_t\}$  based on input  $s_t$ , resulting in a reward  $r_t$ . The objective is to derive the optimal policy  $\pi_\theta^*$  that maximizes the expected cumulative reward  $G_t = \sum_{\tau=t}^T \gamma^{\tau-t} r_\tau$ , where  $\gamma$  denotes the discount factor. The optimal policy  $\pi_\theta^*$  must demonstrate robust performance across all possible scenarios, extending beyond the training environment.

## IV. METHOD

The proposed navigation framework combines a deep reinforcement learning backbone with scenario augmentation to achieve robust generalization. The framework of scenario augmentation is shown in Fig. 1. During navigation, when the agent receives an observation in simulation, the observation scaling module maps it to an imagined observation, which is then processed by the policy network to generate an imagined action. This imagined action is subsequently transformed by policy scaling back into an executable action in the simulation environment. This bidirectional mapping between real and imagined spaces enables the agent to learn from diverse scenarios while operating in a single physical environment.

### A. Learning Navigation with SAC

Once the navigation problem is formulated as a decision-making process, DRL algorithms can be directly applied to identify the optimal policy. The DRL algorithm employed in this paper is the delayed soft actor critic (SAC) [32], which incorporates the delayed policy updating technique from twin delayed DDPG (TD3) [33] to stabilize the training process of SAC.

1) *Neural network architecture:* The neural network architecture for delayed SAC is presented in Fig. 3, wherein the policy network, value network, and two Q networks are parameterized by  $\theta, \psi, \phi_1, \phi_2$ , respectively. Each network

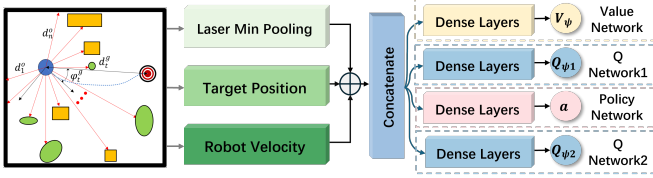


Fig. 3. SAC Neural network architecture.

consists of three hidden dense layers, which exhibit superior generalization capabilities compared to convolutional layers [2]. To optimize computational efficiency, the original laser scan data (1080 laser beams) undergoes 1D minimum down-sampling, reducing the dimensionality to  $N$  values ( $N = 30$ ). The computation of each down-sampled value  $o_{\min}^i$  is defined as:

$$d_{\min,i}^o = \min(d_{i \cdot k + 1}^o, d_{i \cdot k + 2}^o, \dots, d_{i \cdot k + k - 1}^o) \quad (1)$$

where  $i$  denotes the index of the down-sampled laser scans, and  $k$  represents the down-sampling window length ( $k = 36$ ). The state vector  $s$ , comprising down-sampled laser scans, relative goal position, and robot velocities, is processed by the policy network and value network to compute action  $a = \pi_\theta(s)$  and value function  $V_\psi(s)$ , respectively. The two Q networks take  $s$  and  $a$  as input and return Q values  $Q_{\phi_1}(s, a)$  and  $Q_{\phi_2}(s, a)$ . This implementation employs a squashed Gaussian SAC policy, constraining the sampled actions to the interval  $[-1, 1]$ . During the training process, the sampled action  $a_{sam}(s|\theta)$  from the squashed Gaussian policy is computed as:

$$a_{sam}(s|\theta) = \tanh(\mu_\theta(s) + \sigma_\theta(s) \odot \zeta) \quad (2)$$

where  $\mu_\theta(s)$  and  $\sigma_\theta(s)$  denote the mean and standard deviation of the Gaussian policy, and  $\zeta \sim \mathcal{N}(0, 1)$ .

2) *Reward function*: The reward function for robot navigation incorporates two primary components: a positive reward  $r_{reach}$  incentivizing goal-reaching behavior and a negative reward  $r_{crash}$  penalizing collisions. Given that these reward signals occur sparsely during training, we implement an additional dense reward component, following approaches in [2], [8], [9], defined as:

$$r_t^{\text{dense}} = \begin{cases} r_{reach}, & \text{if reaches the goal,} \\ r_{crash}, & \text{if collides,} \\ c_1 (d_t^g - d_{t+1}^g), & \text{otherwise.} \end{cases} \quad (3)$$

where  $c_1$  represents a scaling coefficient. Subsequently, the reward function proposed in [9], [34] is designated as the dense reward. The dense reward function facilitates training convergence by incentivizing progressive movement toward the target through immediate reward optimization. Nevertheless, this dense component may contradict the time-optimal trajectory objective, potentially inducing suboptimal policy convergence [9]. The elimination of the dense component yields a sparse reward function that only provides feedback at the terminal states, as expressed in Equation (4).

$$r_t^{\text{sparse}} = \begin{cases} r_{reach}, & \text{if reaches the goal,} \\ r_{crash}, & \text{if collides.} \end{cases} \quad (4)$$

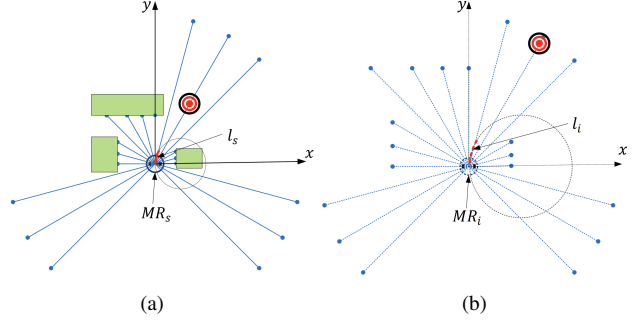


Fig. 4. Overview of scenario augmentation. (a) Robot in simulated space. (b) Robot in imagined space.

The sparse reward function poses significant challenges in learning navigation policies, as positive rewards are exclusively obtained upon goal achievement. Subsequently, we examine the impact of both reward formulations on the agent's generalization capabilities.

### B. Scenario Augmentation

Conventional robot simulators, such as Stage\_ROS, Gazebo, and V-REP [35], maintain a static scenario layout after initial world loading. Existing methodologies for multi-scenario navigation training primarily utilize a curriculum-learning paradigm, wherein agents are initially trained in simplified environments before progressing to more complex scenarios. However, the development of diverse training scenarios demands considerable resources, constraining the available scenario quantity. Goodfellow et al. established that model generalization capability correlates directly with training data diversity [36]. We propose scenario augmentation as an efficient methodology for generating diverse laser-based navigation environments, enabling infinite scenario variations while preserving the original physical layout. The proposed framework (Fig. 4) encompasses two primary stages: 1) observation scaling, which transforms simulated robot observations into scaled representations (imagined observations), and 2) policy scaling, which converts network-generated imagined velocities back to realistic robot velocities. We denote the simulated mobile robot as  $MR_s$  and its imagined counterpart as  $MR_i$ . The implementation of these augmentation stages is elaborated as follows.

1) *Observation-Scaling*: The observation-scaling process transforms current observations into their corresponding imagined representations. Fig. 4a illustrates  $MR_s$  executing a goal-reaching navigation task in the simulation environment. The observation is defined as  $s_s = \{s_s^{dd}, s_s^{di}\}$ , where  $s_s^{dd} = \{o_s, v_s, d_s^g\}$  denotes distance-dependent observations, and  $s_s^{di} = \{\omega_s, \varphi_s^g\}$  denotes the distance-independent observations. For each episode initialization, we introduce a scaling factor  $\rho$ , defined as the ratio of the dimension of the imagined space to the dimension of the simulated space, which is sampled and applied to the distance-dependent observation  $s_s^{dd}$ . Specifically, all the distance-dependent observations are amplified by a factor of  $\rho$ , while the distance-independent observations remain unchanged. Accordingly,

---

**Algorithm 1:** Learning robot navigation with Scenario Augmentation
 

---

```

1 Initialize policy parameters  $\theta$ , Q-value function
  parameters  $\phi_1, \phi_2$ , value function parameter  $\psi$ ,
  empty replay buffer  $\mathcal{B}$ ;
2 while not converge do
3   Initialize step counter  $T$ ;
4   Sample scenario scaling factor  $\rho$  with Eq. (12);
5   while not terminate do
6     Obtain observation  $s_s$  in simulation, calculate
      imagined observation  $s_i$  with Eq. (10);
7     Sample imagined velocities  $a_i \sim \pi_\theta$ ;
8     Calculate the velocities  $a_s$  with Eq. (11) and
      execute it in simulation;
9     Obtain next observation  $s'_s$ ;
10    Calculate  $s'_i$ , reward  $r$  and the terminal signal
       $d_i$ ;
11    Store  $\{s_i, a_i, r, s'_i, d_i\}$  in replay buffer  $\mathcal{B}$ ;
12     $T \leftarrow T + 1$ 
13  end
14  for  $t = 1$  to  $T$  do
15    Sample a minibatch from replay buffer  $\mathcal{B}$ ;
16    Update  $\phi_1, \phi_2, \psi$ ;
17    if  $t \bmod 2 = 0$  then
18      | Update  $\theta$ ;
19    end
20  end
21 end

```

---

the resulting imagined observations  $s_i$  are as follows:

$$s_i = \{\min\{\rho s_s^{dd}, \mathcal{T}(s_s^{dd})\}, s_s^{di}\} \quad (5)$$

where  $\mathcal{T}(\cdot)$  is a threshold function, and  $\mathcal{T}(s_s^{dd})$  returns the upper limits of all the elements in  $s_s^{dd}$ . The imagined observation, as shown in Fig. 4b, is different from the current observation and cannot be seen in the original training scenario.

2) *Policy-Scaling*: The policy-scaling process determines the simulated robot's action vector  $a_s$ . Given imagined observation  $s_i$  as input, the policy network returns the imagined velocities  $a_i = \pi_\theta(s_i) = \{v_\theta(s_i), \omega_\theta(s_i)\}$ . Following the dynamic window approach (DWA) [37], the robot is assumed to move with constant velocities within a control cycle, the generated one-step trajectory  $l_i$  of  $MR_i$  is a circular arc (shown in Fig. 4b). As the dimension of imagined space is  $\rho$  times that of the simulated space, the length of the simulated robot's trajectory  $l_s$  should be the same as the length of  $l_i$  after being amplified by a factor of  $\rho$ , while maintaining identical radians between both trajectories. Accordingly, contrary to the observation-scaling process, the distance-dependent linear velocity is compressed by a factor of  $\rho$ , while the angular velocity remains unchanged. As a result, the velocity  $a_s$  should be:

$$a_s = \left( \frac{v_\theta(s_i)}{\rho}, \omega_\theta(s_i) \right) \quad (6)$$

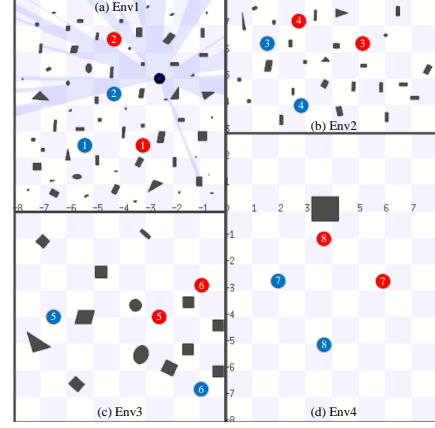


Fig. 5. Simulation environments. (a) Training environment (Env1). (b)-(d) Testing environments (Env2-4).

Through the integration of observation-scaling and policy-scaling mechanisms, the navigation agent accesses observations beyond those available in the original simulation environment. The continuous nature of scaling factor  $\rho$  enables the generation of theoretically infinite unique imagined scenarios.

### C. Learning Navigation with Scenario Augmentation

The proposed scenario augmentation can be easily incorporated into the learning framework for robot navigation. The pseudo-code of learning robot navigation with scenario augmentation is provided in Algorithm 1. At the beginning of each episode, the scenario scaling factor is sampled as follows:

$$\rho = \begin{cases} 1.0, & \epsilon \geq P \\ U[1.0, M], & \epsilon < P \end{cases} \quad (7)$$

where  $\epsilon \sim U[0, 1]$ ,  $P$  denotes the scenario augmentation probability threshold, and  $M$  represents the scaling factor's upper bound. This formulation enables navigation in both simulated and imagined scenarios, while the scaling factor's upper bound  $M$  regulates the probability of empty scenario exploration. During each episode, simulation observations  $s_r$  are transformed into imagined observations  $s_i$  via the scaling factor according to Eq. (5). The DNN controller generates imagined action  $a_i$  based on policy  $\pi_\theta$ , which is then transformed to real action  $a_r$  through Eq. (6) for simulation execution. Following state transition,  $MR_r$  obtains subsequent observation  $s'_r$ , which is transformed into imagined observation  $s'_i$ . The system computes reward  $r_i$  and terminal signal  $d_i$  for the imagined transition, storing the transition tuple  $\{s_i, a_i, r_i, s'_i, d_i\}$  in replay buffer  $\mathcal{B}$ . Episode termination occurs upon destination achievement, collision detection, or reaching maximum step count. The system then performs minibatch training to update all trainable parameters. Network updates are executed  $T$  times for value and Q networks (where  $T$  denotes total episode steps), while the policy network undergoes  $T/2$  updates utilizing delayed update optimization.

## V. EXPERIMENTS

### A. Model training

To evaluate the efficacy of the scenario augmentation method, we conducted systematic comparisons with multiple baseline approaches:

- **DDPG\_SG**: DDPG with Stochastic Guidance [10] is an advanced method that uses a Proportional-Integral-Derivative (PID) controller and an Obstacle Avoidance (OA) controller, especially in the early stages of training. While DDPG\_SG learns from these controllers over time to improve performance, it still struggles to generate optimal straight-line navigation strategies in open environments, even after training with the PID controller. Instead, the model develops suboptimal behaviors, indicating that training with expert controllers does not always result in transferring their optimal characteristics.
- **SAC with Different Reward Functions**: We implemented two variants:
  - **SAC\_DR**: SAC with Dense Rewards;
  - **SAC\_SR**: SAC with Sparse Rewards.

This comparison examines if performance degradation is caused by the reward function. Dense rewards can speed up training by offering immediate feedback for goal-directed movement, but may lead to suboptimal trajectory learning [9]. In contrast, sparse rewards give feedback only at terminal states, potentially leading to better policy development.

- **SAC\_PreT**: SAC with Pre-trained Networks. This method was trained in Env4 to see if continuous training in similar scenarios is needed to maintain strong performance, even with pre-training. It suggests that while curriculum learning can speed up initial training, it may not guarantee lasting optimal performance without continuous exposure to the environment.
- **SAC\_SAUG**: SAC with Scenario Augmentation (our proposed method). This approach addresses the limitations observed in the above baselines by dynamically adapting to different scenarios while maintaining consistent performance across environments.

Further experimental analysis included the implementation of SAC\_SR.v2 and SAC\_SAUG.v2, developed as Dropout-free versions of SAC\_SR and SAC\_SAUG, respectively. Unlike previous studies that evaluate DRL-agents within a single scenario, this study employs Env1 (Fig. 5a) for training and conducts performance evaluation across four distinct scenarios (Env1-4, Fig. 5a-d). SAC\_PreT utilizes Env4 as the pre-training scenario.

The training process utilizes Stage.ROS, a lightweight simulator designed for robot navigation. In the scenario augmentation process, the simulated robot’s dimensions are scaled by  $1/\rho$  relative to the real robot. This scaling ensures collision-free navigation in the simulated environment corresponds to successful traversal in the imagined scenario. Each episode begins with random robot placement in the unobstructed space of the  $8 \times 8\text{m}^2$  training environment. The

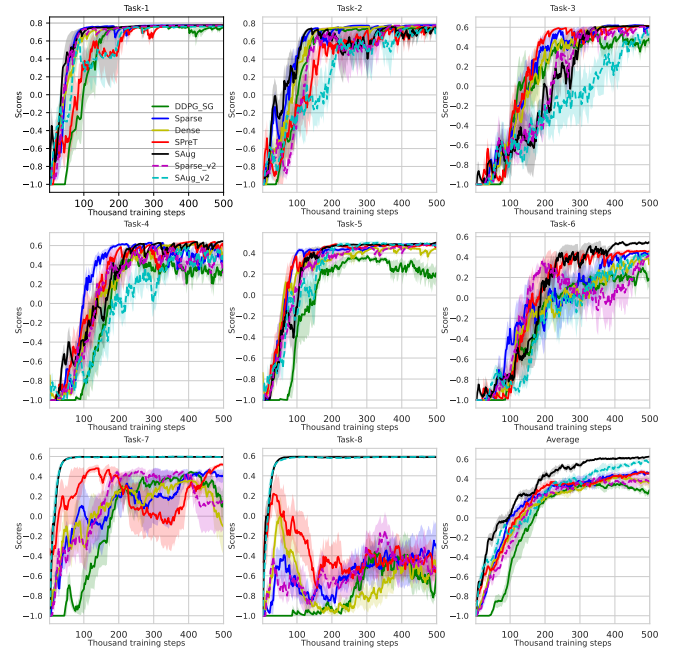


Fig. 6. Learning curves of individual tasks (1-8) and average performance (9).

goal position is randomly selected from unobstructed areas within an  $8 \times 8\text{m}^2$  window centered on the robot and Env1. Training efficiency is enhanced by implementing PID policy [9] for the initial 100 episodes, replacing random exploration. Following this period, the DRL agent executes stochastic actions sampled from the squashed Gaussian policy, initiating network updates. The evaluation procedure involves eight sequential navigation tasks, with start positions and goals indicated by blue and red circles, respectively, in Fig. 5. The performance metric score  $S$ , adopted from [38], is defined as:

$$S = \begin{cases} 1 - \frac{2T_s}{T_{\max}}, & \text{if success,} \\ -1, & \text{otherwise.} \end{cases} \quad (8)$$

where  $T_s$  represents the number of navigation steps required by the agent. This metric combines navigation time and task completion rate to quantify overall performance efficiency. Performance evaluation occurs at 2k-step intervals throughout the one-million-step training process. The training process is replicated five times with distinct random seeds to establish statistical significance. Fig. 6 presents the learning curves with mean scores and variances, indicating that SAC\_SAUG achieves higher performance metrics compared to SAC\_SAUG.v2.

The experimental results reveal significantly enhanced generalization performance through scenario augmentation, as demonstrated by consistent performance across all eight tasks. While all approaches achieved comparable performance scores in the training scenario (Env1, tasks 1 and 2), significant disparities emerged in novel environments. In tasks 7 and 8, approaches without scenario augmentation exhibited substantial performance instability and lower scores, indicating overfitting to the training scenario. No-

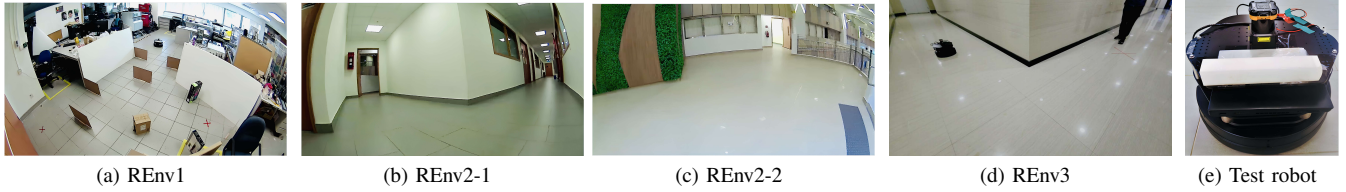


Fig. 7. Real-world testing scenarios. (a) REnv1: Crowded indoor scenario; (b) REnv2-1: Corridor scenario; (c) REnv2-2: Spacious indoor scenario; (d) REnv3: Corridor scenario with pedestrians. (e) The Turtlebot2 robot used for real-world testing.

tably, SAC\_SAUG maintained consistent high scores across all tasks, demonstrating superior generalization capability. The average performance curve shows SAC\_SAUG achieving the highest final score compared to other methods.

SAC\_PreT-trained agents exhibited significant performance limitations, as shown in the learning curves. Despite pre-training in Env4, these agents demonstrated degraded performance in task 7 and task 8, suggesting catastrophic forgetting. The learning curves also reveal that agents trained with dense rewards (SAC\_DR) exhibited more unstable learning patterns and inferior generalization compared to those using sparse rewards (SAC\_SR), particularly evident in tasks 5 through 8 where dense reward curves show higher variance and lower final performance. While both algorithmic choice and reward function design influence generalization, the comparative curves demonstrate that training across varied scenarios through SAC\_SAUG constitutes the most effective approach for enhancing generalization performance.

### B. Navigation in Real-World environment

Real-world environments present complex challenges and inherent uncertainties that computational simulations cannot fully replicate. To evaluate the performance of the five navigation approaches under real-world conditions, we conducted comprehensive experimental trials in physical environments.

1) *Hardware Setup*: Experiments were performed using a Turtlebot2 robot equipped with a Hokuyo UTM-30LX LiDAR sensor, an onboard computer, and a pre-mapped environment for target localization, as shown in Fig. 7e. The LiDAR sensor, with its wide 270° FOV, 30-meter maximum range, and 0.25° angular resolution, served as the primary perception device. Computational processing was executed on a cost-effective i7-7600U CPU laptop without GPU acceleration.

Following an approach similar to [8], target localization was achieved using a pre-mapped testing environment, rather than dedicated sensors such as the UWB system employed in [39]. The environment map was created using the ROS GMapping package, and robot localization within the map was achieved using ROS AMCL. Subsequently, the map was utilized solely for localization purposes.

2) *Testing scenarios and task description*: The real-world performance of the robot was assessed in three distinct environments, as depicted in Fig. 7. These environments, REnv1 (a crowded indoor space), REnv2 (a combination of a corridor section REnv2-1 and a spacious indoor area REnv2-2) and REnv3 (a corridor scenario with pedestrian

TABLE I  
COMPARISON OF NAVIGATION METRICS ACROSS FIVE APPROACHES.

Methods	DDPG_SG	SAC_SR	SAC_DR	SAC_PreT	SAC_SAUG
REnv1					
GR(↑)	3	3	3	3	<b>3</b>
TNN(↓)	34.3	30.6	30.9	32.1	<b>29.4</b>
NC(↓)	0	1	0	0	<b>0</b>
REnv2					
GR(↑)	2	3	4	4	<b>5</b>
TNN(↓)	100.8	83.2	100.0	82.5	<b>53.2</b>
NC(↓)	0	0	0	0	<b>0</b>

traffic), were selected to evaluate the generalization capabilities of the DRL agents under varying levels of environmental complexity. In each environment, the robot was required to navigate from a starting point “S” to a series of target locations, denoted as  $G_i$  and marked by red crosses on the ground (see Fig. 7 and Fig. 9).

#### 3) Experimental Results:

a) *Navigation Performance in Static Environment*: As shown, the robot trajectories and performance metrics are visualized in Figure 9 and Table I, respectively. The metrics in the table are as follows: GR stands for the number of goals reached, TNN represents the total navigation time, and NC represents the number of collisions that occur during the robot’s navigation process. In REnv1, SAC\_SAUG demonstrated a navigation time of 29.4s, yielding a 14.3% improvement over DDPG\_SG (34.3s). All methods navigated to the three target points successfully, with the exception of SAC\_SR, which experienced one collision. Comparative analysis reveals that DDPG\_SG exhibited significant trajectory jerk, indicating control instability, while SAC\_SAUG generated smoother paths with enhanced trajectory optimization and stable motion control.

In the more spacious environment REnv2, SAC\_SAUG exhibited enhanced performance, successfully traversing all 5 target points with a navigation time of 53.2s, representing a 47.2% reduction compared to DDPG\_SG (100.8s). Notably, in the challenging segments between G2-G3 and G3-G4, while other methods exhibited unnecessary detours and occasional failures in reaching target points, SAC\_SAUG consistently generated optimal and smooth trajectories. As shown in Fig. 8e and Fig. 8j, SAC\_SAUG demonstrated

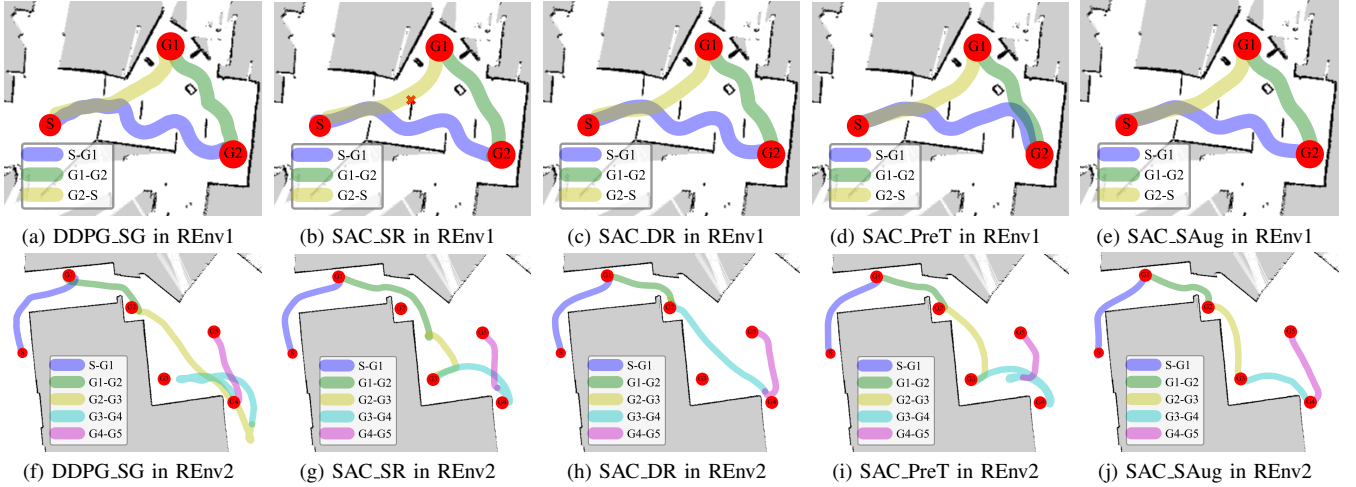


Fig. 8. Robot trajectories for five approaches in REnv1 and REnv2. The experimental videos can be found in the supplementary file.

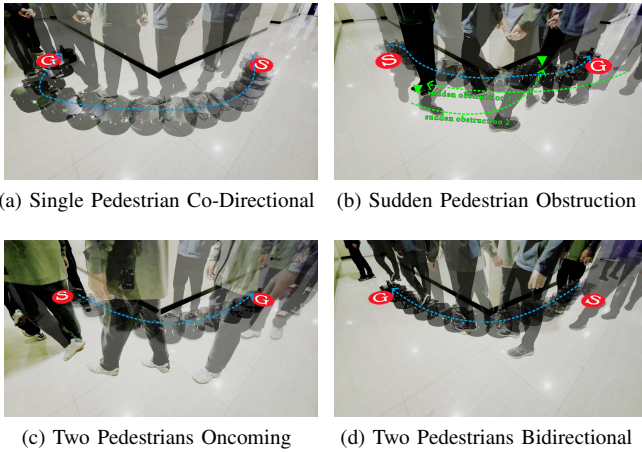


Fig. 9. Real-world robot trajectories in REnv3. The experimental videos can be found in the supplementary file.

superior performance across both environments, featuring near-optimal path planning, smooth motion profiles, and robust environmental adaptability.

#### b) Navigation Performance in Dynamic Scenarios:

To evaluate the method's capability in handling dynamic obstacles, we established four distinct dynamic pedestrian test scenarios: co-directional movement with a single pedestrian, sudden obstruction, counter-directional interaction with two pedestrians, and navigation through opposing pedestrian flows. As shown in Fig. 9, SAC.SAug exhibited effective performance across all scenarios: maintaining optimal following distances and velocity adaptation in co-directional movement, executing efficient evasive maneuvers in obstruction cases, implementing safe navigation between opposing pedestrians, and achieving stable trajectories through pedestrian flows. The experimental results validate the key capabilities of SAC.SAug: adaptive response to dynamic obstacles, efficient goal-reaching behavior, and consistent performance across varied environmental conditions.

## VI. CONCLUSION

In this paper, we introduce scenario augmentation, a novel method to enhance the generalization performance of DRL navigation agents. By mapping observations into an imagined space and remapping actions, this technique facilitates diverse training without altering the actual environment. Through extensive experiments in both simulated and real-world environments, we demonstrated that insufficient diversity of training scenarios is the primary factor limiting navigation performance. Our comparative experiments clearly showed that scenario augmentation significantly improves the agent's adaptability to unfamiliar environments. The real-world experiments further validated the practical value of our approach, with the scenario augmentation method achieving both higher success rates and shorter navigation times compared to baseline approaches. Moreover, it showed excellent obstacle avoidance capabilities and navigation performance in complex dynamic environments.

## REFERENCES

- [1] M. G. Dissanayake, P. Newman, S. Clark, H. F. Durrant-Whyte, and M. Csorba, "A solution to the simultaneous localization and map building (SLAM) problem," *IEEE Transactions on robotics and automation*, vol. 17, pp. 229–241, 2001.
- [2] M. Pfeiffer, S. Shukla, M. Turchetta, C. Cadena, A. Krause, R. Siegwart, and J. Nieto, "Reinforced imitation: Sample efficient deep reinforcement learning for mapless navigation by leveraging prior demonstrations," *IEEE Robotics and Automation Letters*, vol. 3, pp. 4423–4430, 2018.
- [3] Y. LeCun, Y. Bengio, and G. Hinton, "Deep learning," *nature*, vol. 521, pp. 436–444, 2015.
- [4] E. E. Montero, H. Mutahira, N. Pico, and M. S. Muhammad, "Dynamic warning zone and a short-distance goal for autonomous robot navigation using deep reinforcement learning," *Complex & Intelligent Systems*, vol. 10, no. 1, pp. 1149–1166, 2024.
- [5] V. Mnih, K. Kavukcuoglu, D. Silver, A. A. Rusu, J. Veness, M. G. Bellemare, A. Graves, M. Riedmiller, A. K. Fidjeland, and G. Ostrovski, "Human-level control through deep reinforcement learning," *nature*, vol. 518, pp. 529–533, 2015.
- [6] Z. Liu, Q. Liu, L. Tang, K. Jin, H. Wang, M. Liu, and H. Wang, "Visuomotor reinforcement learning for multirobot cooperative navigation," *IEEE Transactions on Automation Science and Engineering*, vol. 19, no. 4, pp. 3234–3245, 2022.

- [7] F. Muratore, M. Gienger, and J. Peters, "Assessing transferability from simulation to reality for reinforcement learning," *IEEE transactions on pattern analysis and machine intelligence*, vol. 43, pp. 1172–1183, 2019.
- [8] L. Tai, G. Paolo, and M. Liu, "Virtual-to-real deep reinforcement learning: Continuous control of mobile robots for mapless navigation," in *2017 IEEE/RSJ International Conference on Intelligent Robots and Systems (IROS)*, 2017, pp. 31–36.
- [9] L. Xie, S. Wang, S. Rosa, A. Markham, and N. Trigoni, "Learning with training wheels: Speeding up training with a simple controller for deep reinforcement learning," in *2018 IEEE International Conference on Robotics and Automation (ICRA)*, 2018, pp. 6276–6283.
- [10] L. Xie, Y. Miao, S. Wang, P. Blunsom, Z. Wang, C. Chen, A. Markham, and N. Trigoni, "Learning with stochastic guidance for robot navigation," *IEEE transactions on neural networks and learning systems*, vol. 32, pp. 166–176, 2020.
- [11] H. Shi, L. Shi, M. Xu, and K.-S. Hwang, "End-to-end navigation strategy with deep reinforcement learning for mobile robots," *IEEE Transactions on Industrial Informatics*, vol. 16, pp. 2393–2402, 2019.
- [12] Y. Zhu, R. Mottaghi, E. Kolve, J. J. Lim, A. Gupta, L. Fei-Fei, and A. Farhadi, "Target-driven visual navigation in indoor scenes using deep reinforcement learning," in *2017 IEEE International Conference on Robotics and Automation (ICRA)*, 2017, pp. 3357–3364.
- [13] Z. Chen, Z. Mandi, H. Bharadhwaj, M. Sharma, S. Song, A. Gupta, and V. Kumar, "Semantically controllable augmentations for generalizable robot learning," *The International Journal of Robotics Research*, p. 02783649241273686, 2024.
- [14] N. Hirose, D. Shah, A. Sridhar, and S. Levine, "ExAug: Robot-conditioned navigation policies via geometric experience augmentation," in *2023 IEEE International Conference on Robotics and Automation (ICRA)*, 2023, pp. 4077–4084.
- [15] K. Cobbe, O. Klimov, C. Hesse, T. Kim, and J. Schulman, "Quantifying generalization in reinforcement learning," in *Proceedings of the 36th International Conference on Machine Learning*, ser. Proceedings of Machine Learning Research, K. Chaudhuri and R. Salakhutdinov, Eds., vol. 97. PMLR, 09–15 Jun 2019, pp. 1282–1289.
- [16] H. Wang, Y. Qiu, Y. Hou, Q. Shi, H.-W. Huang, Q. Huang, and T. Fukuda, "Deep reinforcement learning-based collision-free navigation for magnetic helical microrobots in dynamic environments," *IEEE Transactions on Automation Science and Engineering*, pp. 1–11, 2024.
- [17] H. Van Hasselt, A. Guez, and D. Silver, "Deep reinforcement learning with double q-learning," in *Proceedings of the AAAI conference on artificial intelligence*, vol. 30, no. 1, 2016.
- [18] J. Schulman, F. Wolski, P. Dhariwal, A. Radford, and O. Klimov, "Proximal policy optimization algorithms," *arXiv preprint arXiv:1707.06347*, 2017.
- [19] T. Haarnoja, A. Zhou, P. Abbeel, and S. Levine, "Soft actor-critic: Off-policy maximum entropy deep reinforcement learning with a stochastic actor," in *International conference on machine learning*. PMLR, 2018, pp. 1861–1870.
- [20] Y. Gao, J. Wu, X. Yang, and Z. Ji, "Efficient hierarchical reinforcement learning for mapless navigation with predictive neighbouring space scoring," *IEEE Transactions on Automation Science and Engineering*, vol. 21, no. 4, pp. 5457–5472, 2024.
- [21] A. P. Kalidas, C. J. Joshua, A. Q. Md, S. Basheer, S. Mohan, and S. Sakri, "Deep Reinforcement Learning for Vision-Based Navigation of UAVs in Avoiding Stationary and Mobile Obstacles," *Drones*, vol. 7, no. 4, p. 245, Apr. 2023.
- [22] R. Kirk, A. Zhang, E. Grefenstette, and T. Rocktäschel, "A Survey of Zero-shot Generalisation in Deep Reinforcement Learning," Jan. 2023.
- [23] H. Yang, C. Yao, C. Liu, and Q. Chen, "Rmrl: Robot navigation in crowd environments with risk map-based deep reinforcement learning," *IEEE Robotics and Automation Letters*, vol. 8, no. 12, pp. 7930–7937, 2023.
- [24] R. Cimurs, I. H. Suh, and J. H. Lee, "Goal-driven autonomous exploration through deep reinforcement learning," *IEEE Robotics and Automation Letters*, vol. 7, no. 2, pp. 730–737, 2022.
- [25] Z. Xie and P. Dames, "Drl-vo: Learning to navigate through crowded dynamic scenes using velocity obstacles," *IEEE Transactions on Robotics*, vol. 39, no. 4, pp. 2700–2719, 2023.
- [26] S. Fort, G. K. Dziugaite, M. Paul, S. Kharaghani, D. M. Roy, and S. Ganguli, "Deep learning versus kernel learning: an empirical study of loss landscape geometry and the time evolution of the Neural Tangent Kernel," Oct. 2020.
- [27] G. Valle-Pérez, C. Q. Camargo, and A. A. Louis, "Deep learning generalizes because the parameter-function map is biased towards simple functions," Apr. 2019.
- [28] G. Yang, A. Ajay, and P. Agrawal, "Overcoming the Spectral Bias of Neural Value Approximation," Jun. 2022.
- [29] D. Brellmann, D. Filliat, and G. Frehse, "Fourier Features in Reinforcement Learning with Neural Networks," *Transactions on Machine Learning Research Journal*, 2023.
- [30] B. Cai, C. Wei, and Z. Ji, "Deep reinforcement learning with multiple unrelated rewards for agv mapless navigation," *IEEE Transactions on Automation Science and Engineering*, pp. 1–18, 2024.
- [31] R. Raileanu and R. Fergus, "Decoupling Value and Policy for Generalization in Reinforcement Learning," in *Proceedings of the 38th International Conference on Machine Learning*. PMLR, Jul. 2021, pp. 8787–8798.
- [32] T. Haarnoja, A. Zhou, P. Abbeel, and S. Levine, "Soft actor-critic: Off-policy maximum entropy deep reinforcement learning with a stochastic actor," in *Proceedings of the 35th International Conference on Machine Learning*, ser. Proceedings of Machine Learning Research, J. Dy and A. Krause, Eds., vol. 80. PMLR, 10–15 Jul 2018, pp. 1861–1870.
- [33] S. Fujimoto, H. van Hoof, and D. Meger, "Addressing function approximation error in actor-critic methods," in *Proceedings of the 35th International Conference on Machine Learning*, ser. Proceedings of Machine Learning Research, J. Dy and A. Krause, Eds., vol. 80. PMLR, 10–15 Jul 2018, pp. 1587–1596.
- [34] W. Zhang, N. Liu, and Y. Zhang, "Learn to Navigate Maplessly with Varied LiDAR Configurations: A Support Point-Based Approach," Oct. 2020.
- [35] E. Rohmer, S. P. N. Singh, and M. Freese, "Coppelasim (formerly v-rep): a versatile and scalable robot simulation framework," in *Proc. of The International Conference on Intelligent Robots and Systems (IROS)*, 2013.
- [36] I. Goodfellow, Y. Bengio, and A. Courville, *Deep learning*. MIT press, 2016.
- [37] D. Fox, W. Burgard, and S. Thrun, "The dynamic window approach to collision avoidance," *IEEE Robotics & Automation Magazine*, vol. 4, pp. 23–33, 1997.
- [38] W. Zhang, Y. Zhang, N. Liu, K. Ren, and P. Wang, "Ipaprec: A promising tool for learning high-performance mapless navigation skills with deep reinforcement learning," *IEEE/ASME Transactions on Mechatronics*, vol. 27, no. 6, pp. 5451–5461, 2022.
- [39] T. Fan, P. Long, W. Liu, and J. Pan, "Distributed multi-robot collision avoidance via deep reinforcement learning for navigation in complex scenarios," *International Journal of Robotics Research*, vol. 39, no. 7, pp. 856–892, 2020.